

On the Accuracy of Compressibility Transformations

M. Engin Danis^{*1} and Paul Durbin^{†2}

¹Theoretical Division, Los Alamos National Laboratory, Los Alamos, 87545, USA

²Department of Aerospace Engineering, Iowa State University, Ames, 50011, USA

October 4, 2024

Abstract

This study highlights the importance of satisfying the eddy viscosity equivalence below the logarithmic layer, to deriving accurate compressibility transformations. First, we analyze the ability of known transformations to satisfy the eddy viscosity equivalence and show that the accuracy of these transformation is strongly dependent on this ability. Secondly, in a step-by-step manner, we devise new transformations that satisfy this hypothesis. An approach based on curve fitting of the incompressible Direct Numerical Simulation data for eddy viscosity profiles below the logarithmic layer provides an extremely accurate transformation. That motivates self-contained methods, making use of mixing length formulas, in the inner region.

It is shown that the accuracy of existing transformations can be significantly improved by applying these ideas, below the logarithmic layer. Motivated by the effectiveness of the formulations derived from eddy viscosity equivalence, we introduce a new integral transformation based on Reynolds number equivalence between compressible and incompressible flow. This approach is based on defining a new compressible velocity scale, which affects the accuracy of transformations. Several choices for the velocity scale are tested, and in each attempt, it is shown that the eddy viscosity equivalence plays a very important role for the accuracy of compressibility transformations.

1. Introduction

There has been a growing interest in deriving accurate compressibility transformations in the recent years [12, 13, 5, 6, 9, 10, 1]. The fundamental objective is to relate compressible flow statistics to those of incompressible flow, in order to facilitate analysis, modeling and prediction of compressible wall-bounded turbulence. Unfortunately, the complete set of conditions required to derive accurate compressibility transformations is unknown. This results in appeals to empiricism, while deriving transformations through the introduction of ad-hoc compressibility terms. Hence, many of the existing methods are unable to guide improvement to predictive models. The present study introduces a new condition for transformations, based on the eddy viscosity scaling, which significantly improves accuracy when applied below the logarithmic layer.

Compressibility transformations should be derived by treating the constant stress layer and the outer region separately [10]. In the constant stress layer, Trettel and Larsson argued that profiles of compressible and incompressible shear stresses should collapse under a proper wall-normal coordinate transformation [12]. In fact, that notion of Reynolds stress equivalence was strengthened by several Direct Numerical Simulations (DNS) of zero-gradient hypersonic flow over a flat plate [3, 4, 14, 7]. Denoting the compressible variables by lowercase letters and incompressible

*danis@lanl.gov

†durbin@iastate.edu

variables by uppercase letters, Trettel and Larsson [12] reasoned that if the Reynolds stresses follow wall scaling, and the total stress is constant, viscous stress also scales:

$$\frac{\partial U}{\partial Y} = \frac{\mu}{\mu_w} \frac{\partial u}{\partial y}. \quad (1)$$

As pointed out by Danis and Durbin [2], this results in an eddy viscosity equivalence,

$$\mu_T^+(y) = \mu_{T,i}^+(Y^+), \quad (2)$$

where $\mu_T^+ = \mu_T/\mu$ is the nondimensional compressible eddy viscosity as a function of y and $\mu_{T,i}^+ = \mu_{T,i}/\mu_w$ is the nondimensional incompressible eddy viscosity as a function of Y^+ . Here, $\mu = \mu(y)$ is the local dynamic viscosity and μ_w is its value at the wall $y = 0$. This is in fact a very powerful argument that suggests the compressible and incompressible eddy viscosity profiles should collapse under a proper wall-normal coordinate transformation $y \rightarrow Y$. Thus, the function in (2) need not be determined from incompressible flow: the general idea of wall-scaling using local variables, μ , ρ and τ (the local total stress) is

$$\mu_T = \mu M(Y^+)$$

for some function M .

As a corollary to Equation (2), compressible and incompressible turbulent kinetic energy (TKE) production terms should also be equivalent under the same wall-normal coordinate transformation,

$$\mu P = \overline{\mu \rho u_i'' u_j''} S_{ij} = \tau^2 \mathcal{P}(Y^+) \quad (3)$$

where \mathcal{P} is the wall-scaled production.

The significance of satisfying eddy viscosity equivalence is demonstrated in Figure 1. The transformation of Trettel and Larsson [12] simply sets $Y^+ = y\sqrt{\rho\tau}/\mu$ from the semi-local scaling and uses an integral formula to compute U^+ . It is obvious that eddy viscosity profiles do not collapse on incompressible profiles for $Y^+ > 10$, which generates a mismatch in the y -intercept of the log law corresponding to the transformed velocity profiles. The alternative transformation proposed by Volpiani et al. [13] shows a much better collapse of the eddy viscosity profiles. This directly results in a better collapse of transformed velocity onto incompressible profiles. Despite that success, however, eddy viscosity profiles show incorrect sensitivity to the strong wall cooling of M6Tw025 and M14Tw018 cases. This is also reflected in the nondimensional TKE production profiles, as shown in Figure 2.

In this work, we are mainly focused on the logarithmic layer and below. We propose several accurate transformations for the inner region of wall-bounded hypersonic turbulence. For the sake of completeness, we will also provide the transformed incompressible velocity profiles in the outer region as well, without expecting them to be as accurate. Motivated by this success and inspired by the outer layer scaling approach in [10], we finally introduce a transformation that improves the accuracy in the outer region.

2. Methods and Results

In this section, we introduce several new compressibility transformations for computing the incompressible wall-normal coordinate Y . All of the proposed formulations aim to satisfy eddy viscosity equivalence for $Y^+ \lesssim 40$ and $\partial U/\partial Y = u_\tau/(\kappa Y)$ for a given Von Karman constant κ in the logarithmic layer. The transformed, incompressible velocity U is computed after this step by integrating Equation (1) with respect to the transformed wall-normal coordinate Y .

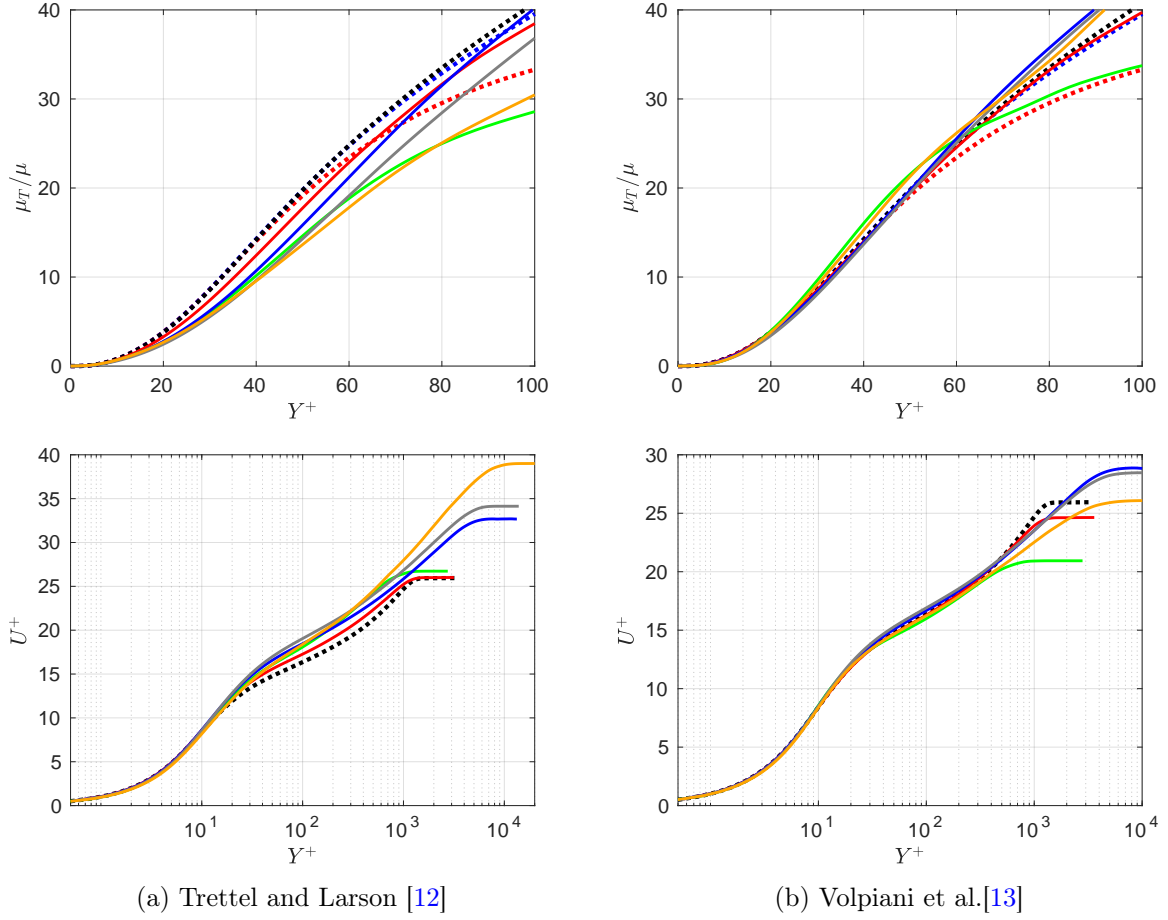


Figure 1: Nondimensional profiles obtained with different compressibility transformations proposed in [12, 13]. Eddy viscosity profiles are on the first row and the transformed velocity profiles are on the second row. Solid lines are compressible DNS [14] test cases: — M2p5, — M6Tw025, — M6Tw076, — M8Tw048, and — M14Tw018. Symbols are incompressible DNS [11] at various Reynolds numbers: ■ $Re_\tau = 492$, ■ $Re_\tau = 974$, and ■ $Re_\tau = 1271$.

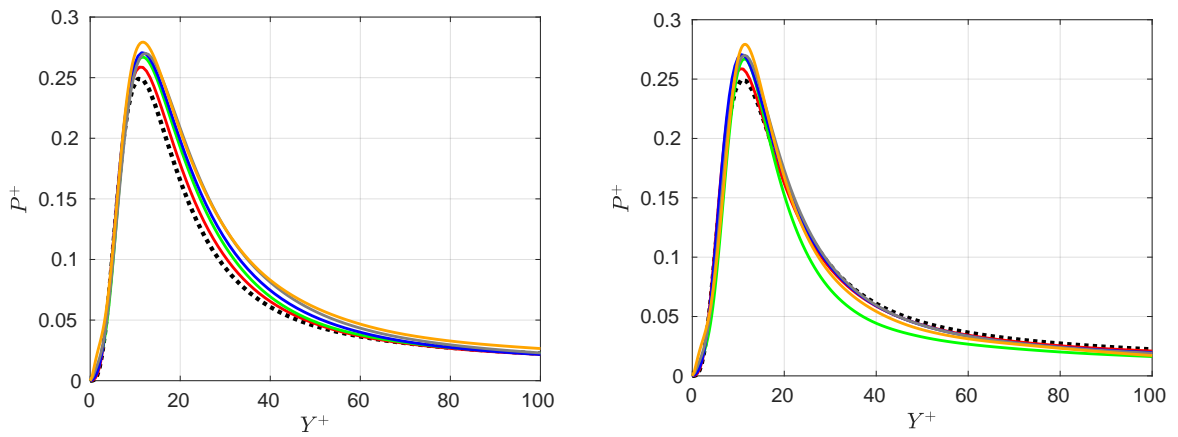


Figure 2: Nondimensional profiles of TKE production obtained with different compressibility transformations proposed in [12, 13]. Legends are the same as those in Figure 1

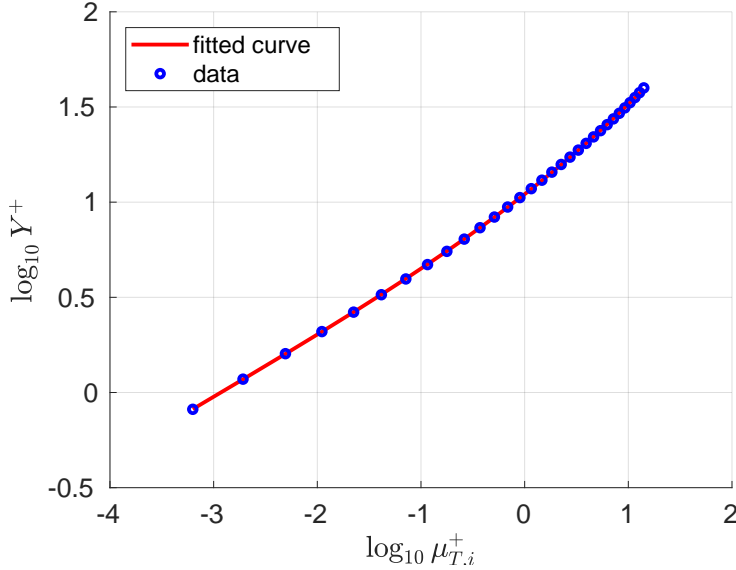


Figure 3: Curve fit for Y^+ vs $\mu_{T,i}^+$ from the incompressible data set [11] up to $Y^+ \lesssim 40$

2.1. Method 1

This transformation is an example designed to illustrate the importance of satisfying the eddy viscosity equivalence below the logarithmic layer. First, we divide the boundary layer into three distinct regions,

$$Y(y) = \begin{cases} Y_1(y), & \text{for } y < y_{log,1} \\ Y_2(y), & \text{for } y_{log,1} \leq y \leq y_{log,2} \\ Y_3(y), & \text{otherwise} \end{cases} \quad (4)$$

Here, $y_{log,1}$ is a representative lower bound for the logarithmic layer and its estimation will be discussed later. The upper bound for the logarithmic layer is denoted by $y_{log,2}$, and for simplicity, it is determined by $y_{log,2} = 0.2\delta_{99}$, where δ_{99} is the standard boundary layer thickness and available in the compressible DNS data set.

To determine $Y_1(y)$ below the logarithmic layer, we follow a straightforward approach and compare $\mu_T^+(y)$ from a compressible DNS to $\mu_{T,i}^+(Y)$ from an incompressible DNS. Since the eddy viscosity equivalence implies $\mu_T^+ = \mu_{T,i}^+$, there exists a one-to-one mapping between Y_1 and y such that

$$Y_1^+ = Y_1^+(\mu_{T,i}^+) = Y_1^+(\mu_T^+(y)) = Y_1^+(y) \quad (5)$$

This one-to-one mapping can be obtained by considering a curve fit in the form of $Y^+ = Y^+(\mu_{T,i}^+)$ from an available incompressible DNS data set. For example, the curve fit

$$\log_{10} Y_1^+ = 4.7896 x^4 + 7.1834 x^3 + 4.0672 x^2 + 4.25 x + 1.0417 \quad (6)$$

is shown in Figure 3 for the data set in [11] for $Y^+ \lesssim 40$ with at least 95% confidence, where $x = (\log_{10} \mu_{T,i}^+) / 10$. The compressible DNS provide $\mu_T(y) = -\overline{\rho u'' v''} / (\partial u / \partial y)$. Following Equation (2), this was substituted into Equation (6) to give $Y_1(y)$ directly.

In the logarithmic region, we simply assume that the incompressible velocity profile follows the log-law

$$\frac{\partial U}{\partial Y} = \frac{u_\tau}{\kappa Y(y)} \quad (7)$$

Using the velocity gradient assumption in Equation (1), an analytical relation for $Y(y)$ is obtained

$$Y_2(y) = \frac{u\tau}{\kappa} \left(\frac{\mu_w}{\mu} \right) \left(\frac{\partial u}{\partial y} \right)^{-1} \quad (8)$$

For the outer-region, a reasonable velocity transformation is obtained by setting

$$Y_3(y) = \left(\frac{\mu_w}{\mu} \right) \left(\frac{\rho}{\rho_w} \right)^{1/2} y, \quad (9)$$

Note that this is equivalent to $Y_3^+ = y^*$, where y^* is the wall-normal coordinate normalized by the semi-local scaling.

The formulation of Method 1 is completed by approximating the lower bound of the logarithmic layer as

$$y_{log,1} = \arg \min_{10 \leq Y_1^+ \leq 50} |Y_1(y) - Y_2(y)| \quad (10)$$

Figure 4 shows the transformed profiles of eddy viscosity, velocity and TKE production. Below the logarithmic layer, the eddy viscosity profiles collapse onto the incompressible profiles. There are kinks while switching from Y_2 to Y_3 , but this is the region where the eddy viscosity equivalence is no longer sought. Recall that the intent of this example is to illustrate the effect of satisfying the eddy viscosity scaling, which is obvious in the transformed velocity profiles in most of the logarithmic layer and below. The compressible profiles are almost indistinguishable as they collapse perfectly onto the incompressible velocity profile in this region. This success is reflected in the relative errors of the transformed velocity, as reported in Table 1. While the transformation presented in Volpiani et al. [13] enjoys an accuracy with errors less than 3.5 %, errors of Method 1 consistently remains less than 0.65 %. Figure 4c also shows a remarkable success in collapsing the compressible TKE production profiles on the incompressible profiles for $Y^+ \leq 100$, which is the best performance reported in the literature so far, to the best of our knowledge. The transformed wall-normal coordinates are compared in Figure 4d. In the adiabatic supersonic case M2p5, the transformed coordinate is below the incompressible line, suggesting that higher Mach numbers push the transformed coordinates further below the incompressible line. A comparison of M6Tw025 and M6Tw076 suggests an opposite effect of wall cooling, as M6Tw025 is closer to the incompressible line. This is supported by the collapse of M6Tw076 onto M8Tw048. In that, high Mach number effects may have been balanced by higher cooling rates in M8Tw048 when collapsing on M6Tw076. The opposite effects of increasing Mach numbers and wall cooling has long been recognized in the literature [8]. In this case, it might be argued that Mach number effects in M14Tw018 play a more prominent role for the transformation than the those of the strong wall cooling, as $Y(y)$ profile is further below M6Tw076 and M8Tw048.

Case	Trettel and Larsson [12]	Volpiani et al. [13]	Present Study (Method 1)
M2p5	5.61	0.83	0.65
M6Tw025	9.60	1.84	0.14
M6Tw076	11.93	2.07	0.65
M8Tw048	15.95	3.51	0.65
M14Tw018	12.86	3.16	0.48

Table 1: Relative errors (percent) of transformed velocity profiles in the inner layer for $y \leq 0.2\delta_{99}$.

2.2. Method 2

This method considers a transformation of the form:

$$Y(y) = \begin{cases} Y_1(y), & \text{for } y < 0.2\delta_{99} \\ Y_2(y), & \text{otherwise} \end{cases} \quad (11)$$

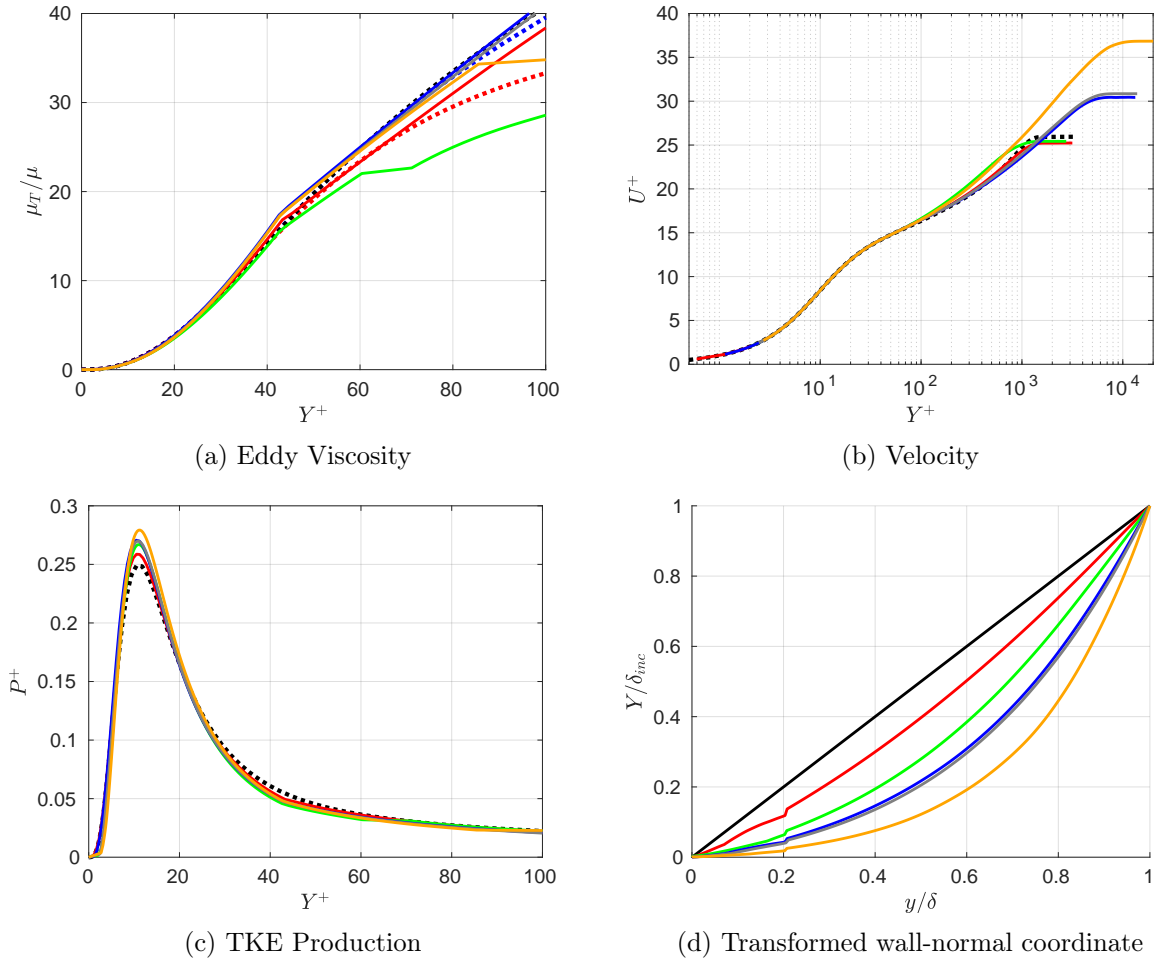


Figure 4: Transformed Profiles with Method 1. Solid black line is for $Y/\delta_{inc} = y/\delta$ and other legends are the same as those in Figure 1.

Instead of curve fitting as in the previous method, this method employs an incompressible mixing length model and Van Driest damping, to satisfy the eddy viscosity hypothesis and log-law in the inner layer for $y < 0.2\delta_{99}$. The incompressible mixing length model is defined as

$$\mu_{T,i}^+ = \frac{\rho_w}{\mu_w} \ell_m^2 \frac{\partial U}{\partial Y}, \quad (12)$$

where ℓ_m is the mixing length. Using the velocity gradient hypothesis Equation (1), the mixing length model becomes

$$\mu_{T,i}^+ = \frac{\rho_w \mu}{\mu_w^2} \ell_m^2 \frac{\partial u}{\partial y}. \quad (13)$$

Next, we invoke the Van Driest damping for an incompressible flow

$$\ell_m = \frac{\mu_w}{\rho_w u_\tau} \kappa Y_1^+ \left(1 - \exp\left(-\frac{Y_1^+}{A^+}\right) \right), \quad (14)$$

and set $\kappa = 0.41$ and $A^+ = 26$. Rewriting the eddy viscosity equivalence in the form $\mu_T^+ - \mu_{T,i}^+ = 0$ and substituting Equation (14) in Equation (13)

$$\mu_T^+ - \left(\frac{\mu}{\rho_w u_\tau^2} \right) \left[\kappa Y_1^+ \left(1 - \exp\left(-\frac{Y_1^+}{A^+}\right) \right) \right]^2 \frac{\partial u}{\partial y} = 0. \quad (15)$$

The premise of scaling is that $u(y)$ is given, and proper scaling should collapse it onto $U(Y)$, via Equation (1): hence, $\rho, \mu, \partial u / \partial y$ are known from the DNS data set and substituting

$$\mu_T^+ = \frac{\tau_w}{\mu \partial u / \partial y} - 1 \quad (16)$$

in Equation (15) provides a closed equation for the transformation $Y_1(y)$. This makes Equation (15) a nonlinear equation for Y_1 , which can easily be solved using Newton's method. Finally, Method 2 is completed by setting Y_2 using the semi-local scaled y^* as in the previous example in the outer region for $y \geq 0.2\delta_{99}$.

Figure 5 shows the transformed profiles. The present transformed compressible eddy viscosity profiles matches the incompressible profiles for $Y^+ \gtrsim 40$ with a reasonable agreement for all Mach numbers and it does not show sensitivity to wall cooling effects like the transformation of Volpiani et al. [13]. It is worth emphasizing that we used the incompressible Van Driest damping parameters without any additional compressibility treatments in this region. The performance of the transformed velocity is slightly worse than Method 1 with a maximum relative error of 1.93% in the inner layer, which is still better than Volpiani et al. [13]. Recall that Y in the inner region –including the logarithmic layer– was computed by a nonlinear Van Driest damping formulation. This approach produced excellent collapse of compressible TKE production profiles to incompressible profiles as shown in Figure 5c. Similar to the previous Method, Figure 5d shows a similar behavior of the transform wall-normal coordinate profiles.

2.3. Method 3 (modified Volpiani transformation)

The previous examples show the significance of satisfying the eddy viscosity equivalence below the logarithmic layer. This gives rise to the question whether existing transformations can be improved by integrating them with this hypothesis. In this example, we present a modified Volpiani transformation. It uses the incompressible mixing length model and Van Driest damping below the logarithmic layer as described in Method 2. Above this region, it sets Y from the transformation of Volpiani et al. [13]:

$$Y(y) = \begin{cases} Y_1(y), & \text{for } y < y_{log,1} \\ Y_2(y), & \text{otherwise} \end{cases} \quad (17)$$

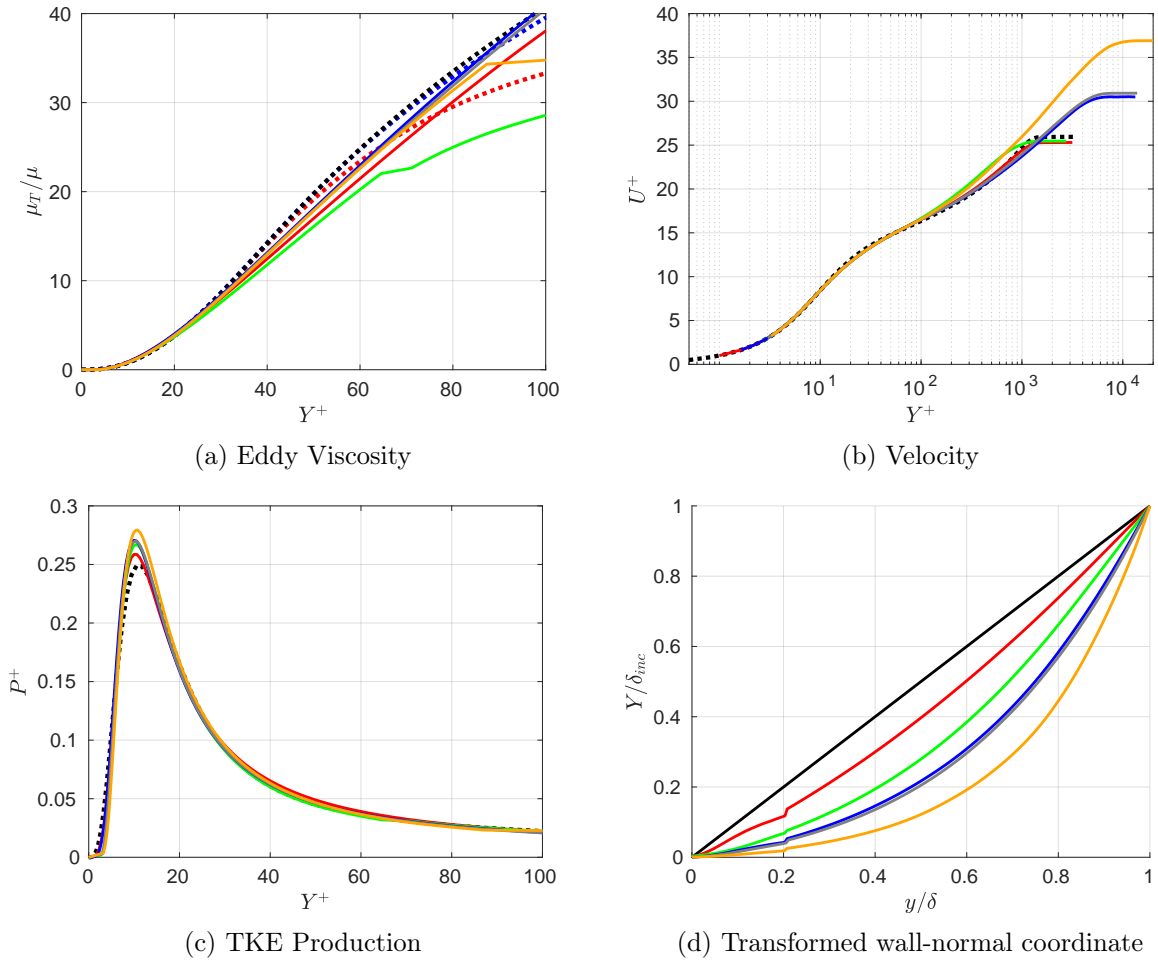


Figure 5: Transformed Profiles with Method 2. Legends are the same as those in Figure 4.

Here, $y_{log,1}$ is computed as in Method 1 and the transformation of Volpiani et al. [13] is modified as

$$Y_2(y) = Y_1(y_{log,1}) + \int_{y_{log,1}}^y \left(\frac{\rho}{\rho_w} \right)^{1/2} \left(\frac{\mu_w}{\mu} \right)^{3/2} dy' \quad (18)$$

Note that the lower bound of this transformation is different from that in [13]. In that, it is changed from $y = 0$ to $y = y_{log,1}$ in Method 3. Note also that, compared to previous examples, this transformation does not use y^* to set the transformed coordinate in the outer layer.

The improved performance of the modified Volpiani transformation is shown in Figure 6. The overall performance is quite similar to Method 2 in the inner layer. The compressible Van Driest treatment removed the dependence on cold wall effects for the eddy viscosity profiles and collapsed them onto the incompressible profiles below the logarithmic layer. This resulted in a decrease of maximum relative error in velocity for the Volpiani transformation from 3.5 % to 1.9 % in the inner layer. The accuracy can be improved further by using Method 1 below the logarithmic layer. In that case, the maximum error is decreased to 0.83 %. As in the previous examples, the transform wall-normal coordinate profiles are similar and the transformed TKE production does not display a significant dependence on the Mach number and wall cooling as these profiles are collapsed on the incompressible profiles for $Y^+ \leq 100$.

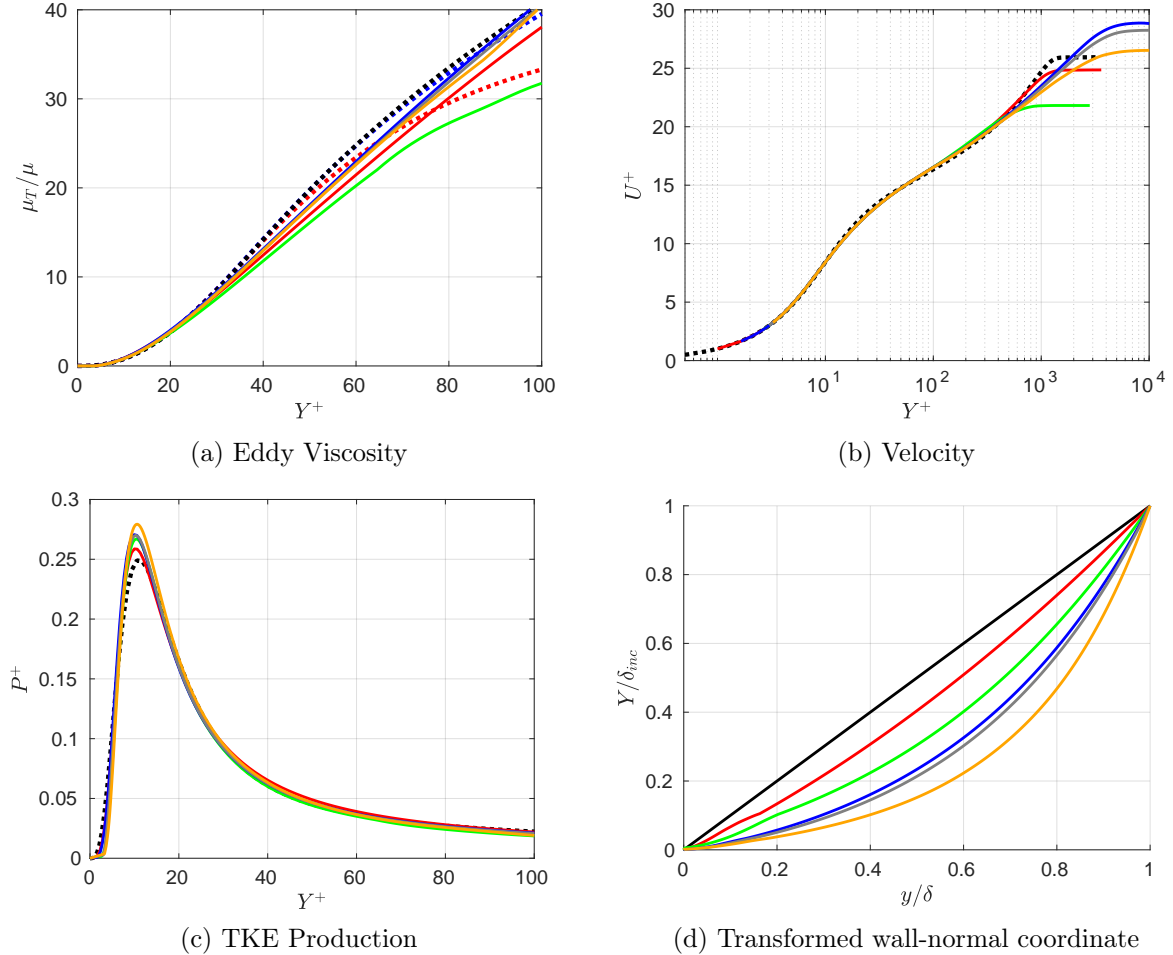


Figure 6: Transformed Profiles with Method 3. Legends are the same as those in Figure 4.

2.4. Method 4 (Reynolds number-based transformation-A)

In this example, we propose a new hypothesis to derive a new compressibility transformation from a claim that, for a compressible Reynolds number definition, there should exist an equivalent incompressible Reynolds number, e.g. $Re_{comp} = Re_{incomp}$, under a suitable compressibility transformation $y \rightarrow Y$. This assumption is mainly motivated by Morkovin's hypothesis, that the dynamics of turbulence is largely a function of the changes in the fluid properties. As a secondary motivation, our considerations can be very useful for deriving a consistent Reynolds number definition for the analysis of hypersonic turbulent boundary layers. Numerous ad-hoc attempts have made to relate compressible boundary layers to incompressible boundary layers in the hopes of finding a proper Reynolds number definition: most prominent examples are Re_τ , Re_τ^* , Re_δ and Re_{δ_2} (see [14] for their definitions).

We choose

$$Re_{inc}(Y) \equiv \int_0^Y \frac{\rho_w u_\tau}{\mu_w} dY' = \frac{\rho_w u_\tau Y}{\mu_w}. \quad (19)$$

Note that at $Y = \delta_i$, where δ_i is the boundary layer thickness of the corresponding incompressible flow, $Re_{inc}(\delta_i)$ reduces to the traditional $Re_\tau = \rho_w u_\tau \delta_i / \mu_w$.

In the same spirit, the compressible Reynolds number can be defined as

$$Re_{comp}(y) = \int_0^y \frac{\rho u_c}{\mu} dy' \quad (20)$$

where u_c is a compressible velocity scale (possibly a function of y) to be determined. Since $\rho \rightarrow \rho_w$ and $\mu \rightarrow \mu_w$ when the compressibility and wall cooling effects disappear as $M \rightarrow 0$ and $T_r \rightarrow T_w$, u_c needs to satisfy $u_c \rightarrow u_\tau$ as a consistency condition.

The Reynolds number equivalence suggests a relation between y and Y . By the fundamental theorem of Calculus, we obtain

$$\frac{dY}{dy} = \left(\frac{\rho}{\rho_w} \right) \left(\frac{\mu_w}{\mu} \right) \left(\frac{u_c}{u_\tau} \right) \quad (21)$$

Note that this is a generalization of the Volpiani transformation [13], which can be easily seen by setting $u_c = \sqrt{(\rho_w/\rho)(\mu_w/\mu)}$.

To derive an analytical expression for u_c in the logarithmic region, we assume the incompressible velocity profile follows the log-law. Differentiating Equation (8) with respect to y and substituting it into Equation (21) give

$$\frac{u_c}{u_\tau} = -\frac{1}{\kappa} \frac{\rho_w}{\rho} \frac{\frac{\partial}{\partial y} \left(\mu \frac{\partial u}{\partial y} \right)}{\mu \left(\frac{\partial u}{\partial y} \right)^2} u_\tau \quad (22)$$

As $M \rightarrow 0$ and $T_r \rightarrow T_w$, we have that $\rho \rightarrow \rho_w$, $\mu \rightarrow \mu_w$, $y \rightarrow Y$, and $\partial_y u \rightarrow u_\tau / \kappa Y$. Then,

$$\frac{u_c}{u_\tau} \rightarrow -\frac{1}{\kappa} \frac{\rho_w}{\rho_w} \frac{\frac{\partial}{\partial Y} \left(\mu_w \frac{u_\tau}{\kappa Y} \right)}{\mu_w \left(\frac{u_\tau}{\kappa Y} \right)^2} u_\tau = 1, \quad (23)$$

which shows consistency in the incompressible limit.

Note that this derivation holds only for the logarithmic layer. Estimating the region below the logarithmic layer is left to the next example and we set Y using the curve fitting approach described in Method 1. In the outer region, we set $u_c = u_\tau$ for simplicity. In summary, Method 4 uses

$$Y(y) = \begin{cases} Y_1(y), & \text{for } y < y_{log,1} \\ Y_2(y), & \text{for } y_{log,1} \leq y \leq y_{log,2} \\ Y_3(y), & \text{otherwise,} \end{cases} \quad (24)$$

where Y_1 is calculated as Method 1 while

$$\begin{aligned}
 Y_2(y) &= Y_1(y_{log,1}) + \int_{y_{log,1}}^y \left(\frac{\rho}{\rho_w} \right) \left(\frac{\mu_w}{\mu} \right) \left(\frac{u_c}{u_\tau} \right) dy' \\
 Y_3(y) &= Y_2(y_{log,2}) + \int_{y_{log,2}}^y \left(\frac{\rho}{\rho_w} \right) \left(\frac{\mu_w}{\mu} \right) dy'
 \end{aligned} \tag{25}$$

Figure 7 shows that Method 4 collapses the compressible eddy viscosity profiles onto incompressible profiles for Y^+ more accurately compared to previous examples. Since the curve fitting is used to match the eddy viscosity for $Y^+ \gtrsim 40$, the transformed velocity profiles have a maximum error of 0.69% in the inner layer for all cases in the compressible DNS data set while the performance in collapsing the TKE production and behavior of the transform wall-normal coordinate profiles are similar to previous examples. Using the Reynolds number equivalence hypothesis, the transformed Reynolds numbers are calculated in Table 2. It is remarkable that the transformed velocity profile of M2p5 Case collapses nicely onto the incompressible DNS profile, while the transformed Reynolds number with $Re_{\tau,incomp} = 1197$ is very close to $Re_{\tau,incomp} = 1271$ of the incompressible DNS data. However, the present study should be considered as accurate only for inner layer transformations. The transformed Reynolds number may not be as accurate in other contexts.

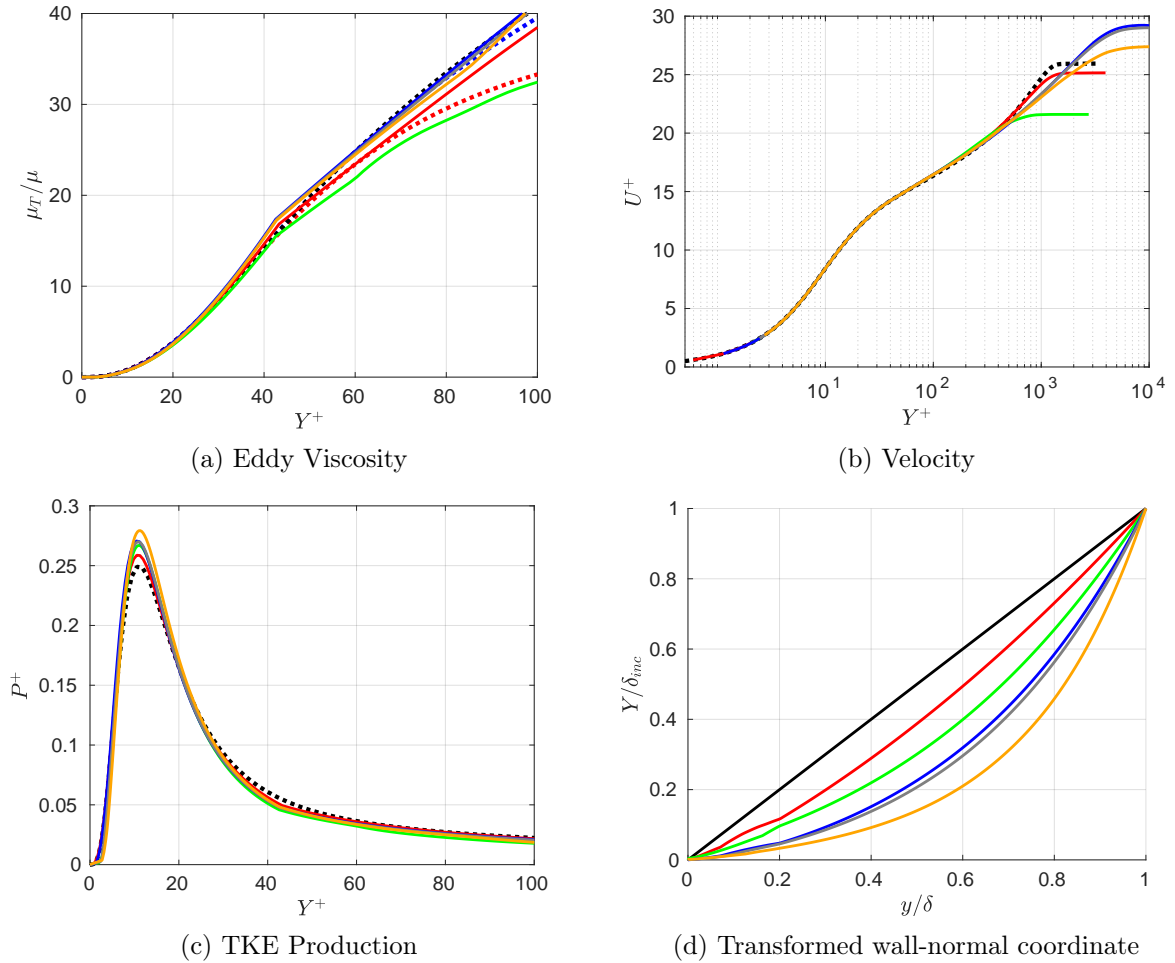


Figure 7: Transformed Profiles with Method 4. Legends are the same as those in Figure 4.

Case	Re_τ [14]	$Re_{\tau, incomp}$
M2p5	510	1197
M6Tw025	450	618
M6Tw076	453	3756
M8Tw048	480	3474
M14Tw018	646	2540

Table 2: Comparison of compressible and transformed Reynolds numbers for Method 4

2.5. Method 5 (Reynolds number-based transformation-B)

In this example, we will explore certain choices for u_c for a transformation of the form:

$$Y(y) = \begin{cases} Y_1(y), & \text{for } y < y_{log,2} \\ Y_2(y), & \text{otherwise,} \end{cases} \quad (26)$$

where

$$\begin{aligned} Y_1(y) &= \int_0^y \left(\frac{\rho}{\rho_w} \right) \left(\frac{\mu_w}{\mu} \right) \left(\frac{u_c}{u_\tau} \right) dy' \\ Y_2(y) &= Y_1(y_{log,2}) + \int_{y_{log,2}}^y \left(\frac{\rho}{\rho_w} \right) \left(\frac{\mu_w}{\mu} \right) dy' \end{aligned} \quad (27)$$

Clearly, a natural choice for the compressible velocity scale u_c can be $u_c = u_\tau$, assuming that the compressible velocity scale is the same the incompressible friction velocity and the changes in the Reynolds numbers are due to the changes in the fluid properties. Another reasonable choice is to set $u_c = u_\tau^*$ where $u_\tau^* = \sqrt{\tau_w/\rho}$ is the semi-local friction velocity. In order to include wall heat transfer, one might set $u_c = u_\tau^* + u_q$, where

$$u_q = \frac{q_w}{\rho C_p T}, \quad q_w = - \left(k \frac{\partial T}{\partial y} \right)_{y=0} \quad (28)$$

and q_w is the heat flux at the wall. A summary of u_c choices is provided in Table 3.

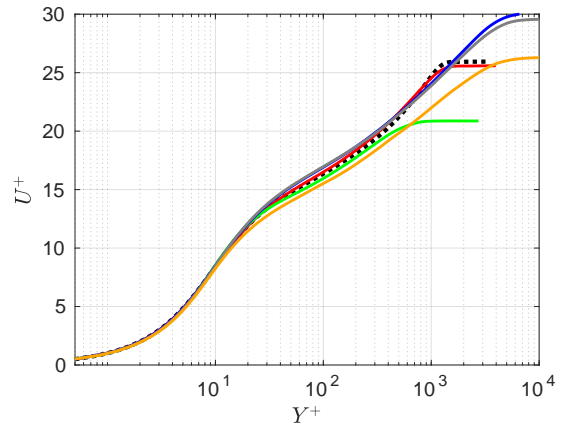
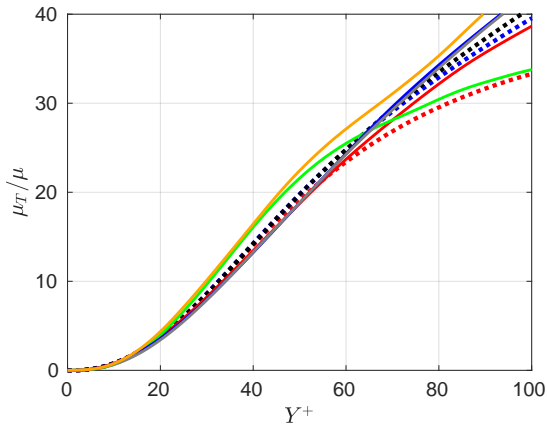
Method	u_c	Maximum velocity error (%)
5a	u_τ	5.13
5b	u_τ^*	12.4
5c	$u_\tau^* + u_q$	4.18

Table 3: Summary of Method 5

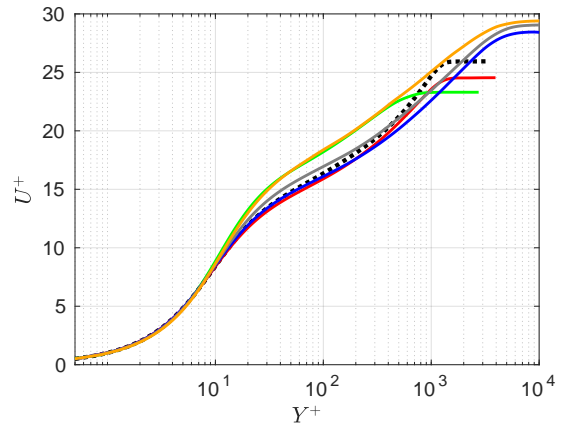
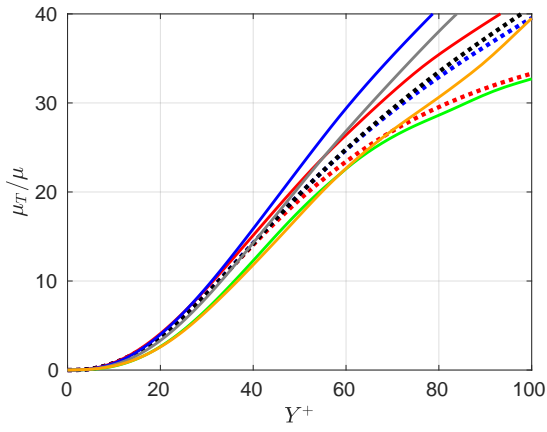
Figure 8 shows the influence of u_c choices on the transformations. Eddy viscosity profiles obtained from Method 5a with $u_c = u_\tau$ have slightly higher sensitivity to wall cooling than the transformation in Volpiani et al. [13], which results in a larger velocity error of 5.13% in the inner layer. Interestingly, Method 5b with $u_c = u_\tau^*$ has a larger variation in eddy viscosity and this causes velocity errors up to 12.4%. By adding u_q , to include wall heat transfer, Method 5c improves the collapse of eddy viscosity profiles for $Y^+ \lesssim 40$, which mostly removes the velocity errors of Method 5b.

2.6. Method 6 (Iterative transformation based on inner/outer scaling)

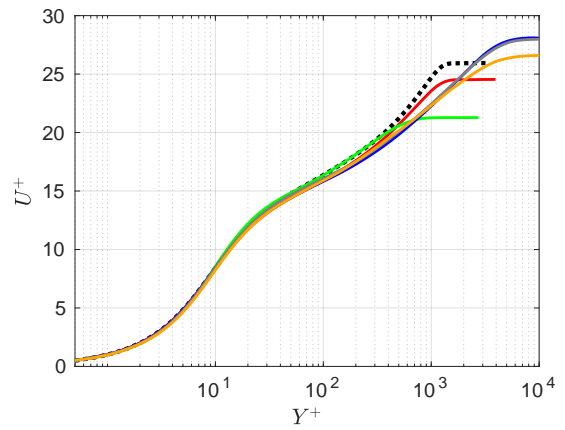
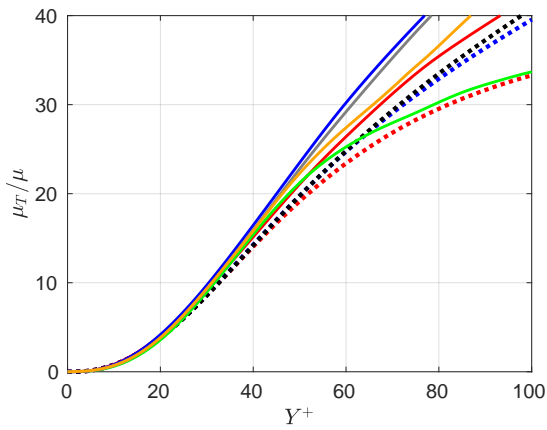
Inspired by [10], the last method transforms the whole boundary layer by using both inner and outer scaling of incompressible flows. For that reason, it deviates from the other approaches.



(a) Method 5a $u_c = u_\tau$



(b) Method 5b $u_c = u_\tau^*$



(c) Method 5c $u_c = u_\tau + u_q$

Figure 8: Transformed Profiles with Method 5. Eddy viscosity is on the left and velocity is on the right. Legends are the same as those in Figure 1.

Unlike [10], however, we propose a transformation via an iterative scheme, without employing additional compressibility treatments for the inner and outer scaling of incompressible flows.

In each iteration, the proposed transformation is determined by

$$Y(y) = \begin{cases} Y_1(y), & \text{for } Y < 0.2\delta_{99,inc} \\ Y_2(y), & \text{for } 0.2\delta_{99,inc} \leq Y \leq \delta_{99,inc} \end{cases} \quad (29)$$

where Y_1 is obtained from the incompressible mixing length model and Van Driest damping, as in Method 2, while the law of the wake with Cole's wake function,

$$U(Y) = \frac{u_\tau}{\kappa} \log\left(\frac{Y u_\tau}{\nu_w}\right) + B u_\tau + 2 \frac{\Pi u_\tau}{\kappa} \sin^2\left(\frac{\pi Y}{2\delta_{99,inc}}\right), \quad (30)$$

is used estimate Y_2 . For present purposes, the wake parameter is the zero-pressure gradient value $\Pi = 0.8 \times (0.5^{3/4})$. The wall-normal derivative of incompressible velocity is given as

$$\frac{dU}{dY} = \frac{u_\tau}{\kappa Y} + \frac{\Pi u_\tau}{\kappa \delta_{99,inc}} \sin\left(\frac{\pi Y}{\delta_{99,inc}}\right) \quad (31)$$

By the velocity scaling (1), we obtain a nonlinear equation for Y_2

$$\frac{u_\tau}{\kappa Y_2} + \Pi \frac{\pi u_\tau}{\kappa \delta_{99,inc}} \sin\left(\frac{\pi Y_2}{\delta_{99,inc}}\right) - \frac{\mu}{\mu_w} \frac{du}{dy} = 0 \quad (32)$$

Since $(\mu/\mu_w)(du/dy)$ is available from a compressible DNS, this relation can be solved by Newton's method for Y_2 .

Note that this transformation does not use incompressible DNS data in its formulation. In addition, unlike the previous approaches where the upper bound of the inner layer is taken from compressible coordinates as $0.2\delta_{99}$, this method sets it from the transformed incompressible coordinate as $0.2\delta_{99,inc} = 0.2Y(\delta_{99})$. The iterations are assumed to be converged when $\delta_{99,inc}$ is sufficiently converged.

Figure 9 shows the profiles of transformed eddy viscosity, velocity and TKE production. Compared to Method 2, Method 6 removes the kinks and results in smooth eddy viscosity profiles due to better matching conditions at $Y = 0.2\delta_{99,inc}$. The velocity profiles are shown only up to the boundary layer edge, as this transformation holds only inside the boundary layer. We observe that the compressible velocity profiles collapse on incompressible profiles accurately, with a maximum error of 1.93%. Note that this error is measured for $y < 0.2\delta_{99}$, which is consistent with the previous cases and also with the fact that the logarithmic layer of the actual incompressible data is shorter compared to that of the transformed versions of M6Tw076, M8Tw048 and M14Tw018 cases. Figure 9d demonstrates the most notable difference of the present method to previous ones. While high Mach numbers push the transform wall-normal coordinate profiles below the incompressible line, all hypersonic cases have similar trends while the profiles of the cold wall cases (M6Tw025 and M14Tw018) almost collapse on the other. This might be because the lower bound of the outer layer is taken from the incompressible state and it is determined iteratively. Larger variations in the material properties due to larger variations in the temperature in these cases might also have been another factor.

3. Conclusion

In this paper, we showed the significance of satisfying the eddy viscosity equivalence below the logarithmic layer for deriving accurate compressibility transformations. We demonstrated that the Trettel and Larsson [12] transformation does not meet this criterion, while the Volpiani transformation [13] is better, except for a slight sensitivity to wall cooling, which makes it a more accurate

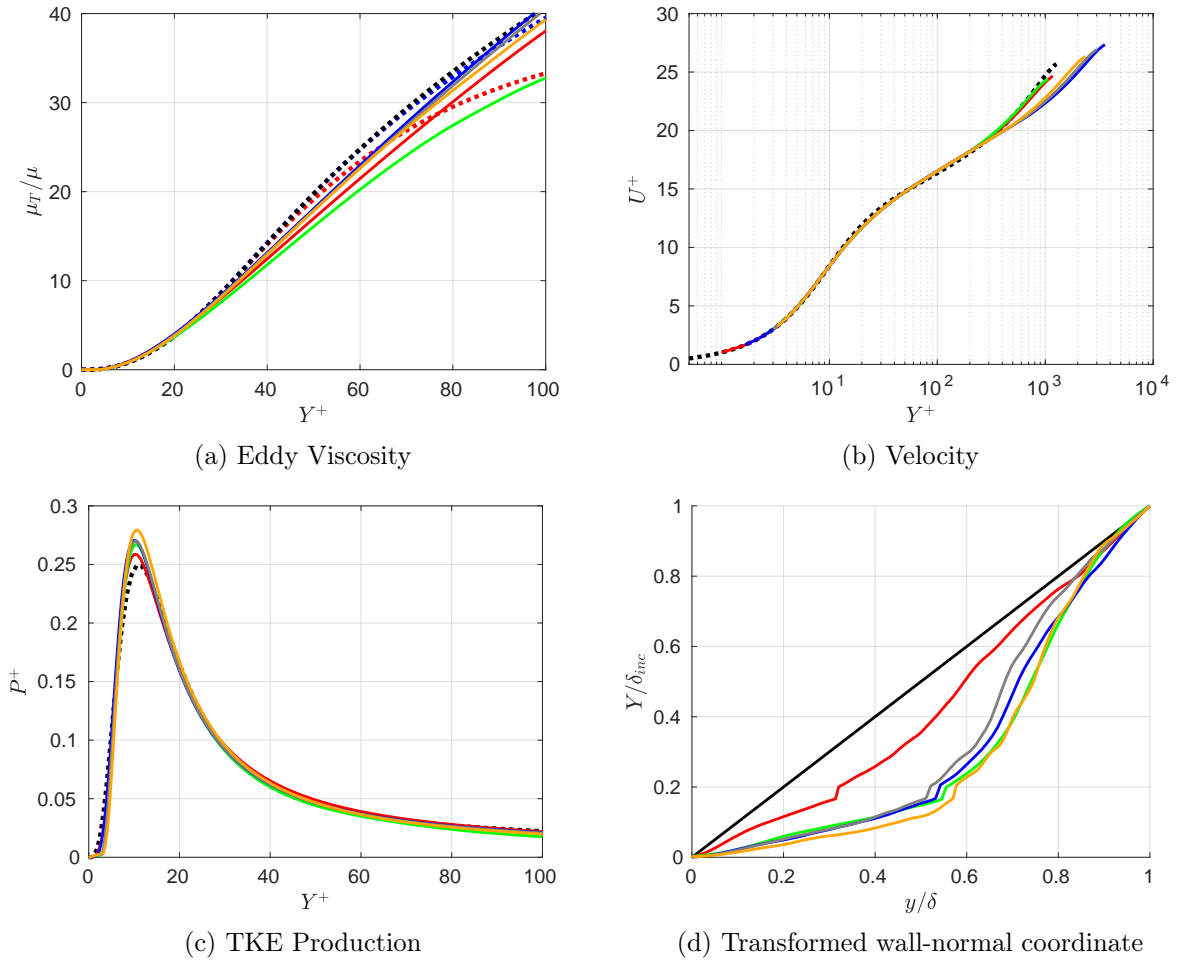


Figure 9: Transformed Profiles with Method 6. Legends are the same as those in Figure 4.

transformation. To remove the dependence on wall-cooling, we introduced two approaches – curve fitting incompressible DNS eddy viscosity profiles and transforming incompressible Van Driest damping. We proposed several new transformations that use these ideas, including one that significantly improves the accuracy of the Volpiani transformation [13]. This success motivated a new integral transformation, which introduced a new compressible velocity scale. We showed that accurate transformations can be obtained by respecting the physics of the turbulence as well as compressibility and wall cooling effects.

Acknowledgments

This work was funded in part by the Office of Naval Research grant #N00014-21-1-2264.

References

- [1] Cheng Cheng and Lin Fu. Mean temperature scalings in compressible wall turbulence. *Phys. Rev. Fluids*, 9:054610, May 2024.
- [2] Mustafa E. Danis and Paul Durbin. Compressibility correction to $k-\omega$ models for hypersonic turbulent boundary layers. *AIAA Journal*, 60(11):6225–6234, 2022.
- [3] L Duan, I Beekman, and MP Martin. Direct numerical simulation of hypersonic turbulent boundary layers. part 2. effect of wall temperature. *Journal of Fluid Mechanics*, 655:419–445, 2010.
- [4] L Duan, I Beekman, and MP Martin. Direct numerical simulation of hypersonic turbulent boundary layers. part 3. effect of mach number. *Journal of Fluid Mechanics*, 672:245–267, 2011.
- [5] Kevin Patrick Griffin, Lin Fu, and Parviz Moin. Velocity transformation for compressible wall-bounded turbulent flows with and without heat transfer. *Proceedings of the National Academy of Sciences*, 118(34), 2021.
- [6] Asif Manzoor Hasan, Johan Larsson, Sergio Pirozzoli, and Rene Pecnik. Incorporating intrinsic compressibility effects in velocity transformations for wall-bounded turbulent flows. *Phys. Rev. Fluids*, 8:L112601, Nov 2023.
- [7] Junji Huang, Gary L Nicholson, Lian Duan, Meelan M Choudhari, and Rodney D Bowersox. Simulation and modeling of cold-wall hypersonic turbulent boundary layers on flat plate. In *AIAA Scitech 2020 Forum*, page 0571, 2020.
- [8] P. G. Huang and G. N. Coleman. Van driest transformation and compressible wall-bounded flows. *AIAA Journal*, 32(10):2110–2113, 1994.
- [9] P.G. Huang, G.N. Coleman, P.R. Spalart, and X.I.A. Yang. Velocity and temperature scalings leading to compressible laws of the wall. *Journal of Fluid Mechanics*, 977:A49, 2023.
- [10] Asif Manzoor Hasan, Johan Larsson, Sergio Pirozzoli, and Rene Pecnik. Estimating mean profiles and fluxes in high-speed turbulent boundary layers using inner/outer-layer scalings. *AIAA Journal*, 62(2):848–853, 2024.
- [11] Philipp Schlatter and Ramis Örlü. Assessment of direct numerical simulation data of turbulent boundary layers. *Journal of Fluid Mechanics*, 659:116–126, 2010.
- [12] Andrew Trettel and Johan Larsson. Mean velocity scaling for compressible wall turbulence with heat transfer. *Physics of Fluids*, 28(2):026102, 02 2016.
- [13] Pedro S. Volpiani, Prahladh S. Iyer, Sergio Pirozzoli, and Johan Larsson. Data-driven compressibility transformation for turbulent wall layers. *Phys. Rev. Fluids*, 5:052602, May 2020.
- [14] Chao Zhang, Lian Duan, and Meelan M Choudhari. Direct numerical simulation database for supersonic and hypersonic turbulent boundary layers. *AIAA Journal*, 56(11):4297–4311, 2018.